OPEN ACCESS

University of BRISTOL

Harper, P. W., & Hallett, S. R. (2015). Advanced numerical modelling techniques for the structural design of composite tidal turbine blades. *Ocean Engineering*, *96*, 272-283. https://doi.org/10.1016/j.oceaneng.2014.12.025

Peer reviewed version

Link to published version (if available):
10.1016/j.oceaneng.2014.12.025

Link to publication record in Explore Bristol Research
PDF-document

10.1016/j.oceaneng.2014.12.025

University of Bristol - Explore Bristol Research
General rights

This document is made available in accordance with publisher policies. Please cite only the published version using the reference above. Full terms of use are available:
http://www.bristol.ac.uk/red/research-policy/pure/user-guides/ebr-terms/

Published in Ocean Engineering 2015; 96. pp 272–283
DOI: 10.1016/j.oceaneng.2014.12.025

ADVANCED NUMERICAL MODELLING TECHNIQUES FOR THE STRUCTURAL DESIGN OF COMPOSITE TIDAL TURBINE BLADES

Paul W. Harper, Stephen R. Hallett

Advanced Composites Centre for Innovation and Science,
University of Bristol, Queen's Building, University Walk, Bristol, BS8 1TR, UK

Corresponding Author: Paul.Harper@bristol.ac.uk

Abstract:

Tidal Stream turbine blades must withstand both extreme one-off loads and severe fatigue loads during their 20-25 year required lifetimes in harsh marine environments. This necessitates the use of high-strength fibre reinforced composite materials to provide the required stiffness, strength and fatigue life, as well as resistance to corrosion, whilst minimising the mass of material required for blade construction and allowing its geometric form to provide the required hydrodynamic performance. Although composites provide superior performance to metals, potential failure mechanisms are more complicated and difficult to predict. A dominant failure mechanism is interfacial failure (delamination) between the composite layers (plies). This paper demonstrates how the development of numerical techniques for modelling the growth of interfacial cracks can aid the design process, allowing the effects on crack growth from potential manufacturing defects and the effect of stacking sequence of composite plies to be analysed. This can ultimately lead to reduced design safety margins and a reduction in the mass of material required for blade manufacture, essential for reducing lifecycle costs. Although the examples provided in this article are specific to tidal turbine blades, the analysis techniques are applicable to all composite structures where fatigue delamination is a primary failure concern.

Keywords: Tidal Energy, Composites, Fatigue, Fracture, Structures

Published in Ocean Engineering 2015; 96. pp 272–283
DOI: 10.1016/j.oceaneng.2014.12.025

Nomenclature

Interface Element Properties:

G_C	Critical Strain Energy Release Rate
K	Interface Element Stiffness prior to damage initiation
σ	Interface Element Stress
σ_{max}	Maximum Interfacial Stress
δ	Interface Element Relative Displacement
δ_e	Interface Element Relative Displacement at damage initiation
δ_f	Interface Element Relative Displacement at final failure

Subscripts *I*, *II* and *m* are used to denote properties under mode I, mode II and mixed mode loading respectively.

Laminate Properties:

E_{11}, E_{22}, E_{33}	Young's Moduli
G_{12}, G_{13}, G_{23}	Shear Moduli
$\nu_{12}, \nu_{13}, \nu_{23}$	Poisson's Ratios

where subscripts 1, 2 and 3 denote the principal material axes.

Miscellaneous:

G_T	Total Strain Energy Release Rate (subscripts I and II are used to denote mode I and mode II components)
P	Load
t	Time
a	Crack Length
N	Number of fatigue cycles
C	Paris Law constant
m	Paris Law exponent

Published in Ocean Engineering 2015; 96. pp 272–283
DOI: 10.1016/j.oceaneng.2014.12.025

1. Introduction

Although estimates of the global resource vary, tidal stream devices could potentially extract significant quantities of energy from a variety of regions where there are fast flowing tidal currents, such as the Pentland Firth, Bay of Fundy, Skagerrak-Kattegat, the Gulf's of Mexico and St Lawrence, rivers such as the Amazon and the Straits of Magellan and Messina (Charlier, 2003). The UK has one of the world's richest resources and recent estimates suggest that tidal stream energy devices could provide approximately 21 TWh/yr of UK electricity (Black and Veatch, 2011), which is equivalent to around 5% of total supply.

There is currently a wide range of tidal stream devices under development, but those closest to commercial deployment are generally open-bladed horizontal axis turbines, such as Marine Current Turbine's SeaGen, Tidal Generation Ltd's Deep Gen and Andritz Hydro Hammerfest's HS1000 (RenewableUK, 2012). Similar to wind turbines, the design lifetime of tidal stream devices will be 20-25 years but there is an even greater incentive for low maintenance requirements due to the harsh, inaccessible, marine environments where they will operate. This makes it vital to fully understand the loads that tidal turbines will experience and to design against potential failure mechanisms.

The cyclic loads experienced by tidal turbine blades are significantly different to those acting on wind turbine blades. Water has a density 832 times that of air and as a result, flapwise bending loads dominate for tidal turbine blades, wheareas for wind turbine blades, centripetal loads dominate due to the low density of air and their relatively high rotational speeds (Fraenkel, 2004). Although tidal turbines are subjected to a predictable tidal current, which varies between two maximum speeds of typically 3-4 m/s in opposite directions over a 12 hour period, short-term variations in load are imposed by wave action and turbulence (e.g. due to sea-bed roughness and temperature effects). This means that in addition to extreme one-off load cases, such as a 50-year extreme wave event, material degradation under cyclic loads (fatigue) is a highly important design consideration (McCann, 2007). The severity of fatigue loads experienced by tidal turbines is both design and site-specific, depending on factors such as the depth of installation, the proximity of the sea-bed and the wave environment (McCann et al., 2008). The acquisition of appropriate experimental data to gain an improved understanding of fatigue loading has received much attention at sites such as the European Marine Energy Centre in Orkney (Droniou and Norris, 2007; Lawrence et al., 2009).

The structure of a typical tidal turbine blade is shown in Figure 1 and consists of a main spar running along the length of the blade, enclosed by a skin to give the blade its hydrodynamic shape. Carbon and glass

Published in Ocean Engineering 2015; 96. pp 272–283
DOI: 10.1016/j.oceaneng.2014.12.025

fibre reinforced composites are currently the favoured materials for these components (Marsh, 2004) due to their high stiffness, strength, and fatigue/corrosion resistance. During manufacture, layers known as plies, which consist of straight, continuous fibres, pre-impregnated with resin, are stacked on top of one another. The resulting stack of plies, known as a laminate, is then heated and cooled in a controlled manner so that the resin forms strong chemical bonds with the fibres and sets to form a rigid structure. The thickness of the blade is tapered from root to tip by incrementally terminating plies along the length of the blade, forming features known as ply drops. The combination of very strong fibres surrounded by a lightweight plastic matrix enables a greater strength and stiffness to weight ratio than is possible using metallic materials. Compared to metals, composites offer the additional advantages of an ability to be moulded into complex shapes and resistance to corrosion. Although the fatigue performance of composites is also generally better than metals, fatigue remains a significant design consideration and is a highly complex failure regime to predict due to the many types of damage mechanism that can occur in fibre reinforced composites. These include cracks developing both within the individual plies of the laminate (intralaminar damage) and often more significantly, along the interfaces between plies (interlaminar damage) (Jones, 1999; Harris, 2003).

Figure 1: A typical tidal turbine blade structure

Although guidelines and standards for the certification of tidal turbine devices have been issued (GL, 2005; DNV 2008), efforts to develop and refine the associated design processes remain ongoing. The structural design process for tidal turbine blades can be divided into three main stages, as shown in Figure 2:

1. Modelling the actual fatigue load spectrum that a tidal turbine blade will be subjected to during its 20-25 year lifetime (Gant and Stallard, 2008). This relies on having reliable data for both the range of mean current speeds and level of flow turbulence at a given site. Specialist software tools such as Garrad Hassan's 'Tidal Bladed' (Bossanyi, 2007) and NREL's 'TurbSim' (Jonkman and Kelley, 2007) have been developed which can model both the hydrodynamic performance and the fatigue load spectrum, based on empirical turbulence data from sites such as the European Marine Energy Centre. Figure 2 (1. Analysis of extreme static and fatigue loads) shows a typical analysis output from GH Bladed where the temporal variation of the bending moment at the blade root consists of both a sinusoidal periodic component due to the harmonic tidal cycle and random short-term variations due to turbulence.

2. Converting this complex fatigue load spectrum to a series of constant amplitude, constant frequency, sinusoidal fatigue loads (Equivalent Fatigue Loads) that cause an equivalent level of material degradation

Published in Ocean Engineering 2015; 96. pp 272–283
DOI: 10.1016/j.oceaneng.2014.12.025

over the turbine lifetime and can be used for design and experimental certification purposes. Figure 2 (2. Generation of simplified fatigue spectrum) shows sets of constant amplitude, sinusoidal fatigue loads that can be used within a numerical simulation to represent the cyclic components of the actual fatigue spectrum. Although this will not account for any variations in damage accumulation due to the sequence in which cyclic loads are applied, modelling the actual temporal fatigue spectrum within an explicit Finite Element simulation, as performed in the current investigation, is not currently feasible (see section 2.1).

3. The application of design and analysis techniques to ensure that the simplified fatigue spectrum will not result in structural failure within the required design lifetime. This is the focus of the current paper and the methods being applied to address this challenge are now discussed in more detail.

Figure 2: The Structural Design Process for Tidal Turbine Blades

For wind turbine blades, extensive experimental studies have been conducted to investigate the effect of cyclic loading on composite material degradation (McGowan et al., 2007) and formal design procedures have been developed to account for these (Sutherland, 1999). However, there remains significant ongoing research into the effects of mean stress and variable amplitude loading on material degradation, which have a significant impact on whether current methods for deriving Equivalent Fatigue Loads are adequate (Sutherland and Mandell, 2004). These issues are equally relevant for tidal turbine blade design and in addition, recent studies have recognised that there is a need for a greater understanding of carbon/glass fibre reinforced composite materials degradation in marine environments. Davies and co-workers at the IFREMER research institute in Brest, France, have investigated the effect of long-term cyclic loading of such materials in sea-water, involving a number of composite material manufacturers (Davies et al., 2013; Boisseau et al., 2013). In addition, a UK project 'New Materials and Methods for Energy Efficient Tidal Turbines (NEW-MMEETT),' funded by the Technology Strategy Board (TSB), has focused on developing more fatigue resistant resins, in conjunction with design techniques for analysing material degradation (TSB, 2008). The studies presented in this paper were conducted through the NEW-MMEETT programme.

In all of this work, a key failure mode under consideration, both under static and fatigue loads, is the growth of cracks along the interfaces between plies, which generally grow from areas of high stress, such as those found at ply drops. Due to the time and cost involved in experimental test programmes that investigate a wide range of ply stacking sequences and ply drop geometries, there has been a strong drive to develop numerical analysis techniques that can aid the design process and reduce the amount of experimental tests that

Published in Ocean Engineering 2015; 96. pp 272–283
DOI: 10.1016/j.oceaneng.2014.12.025

need to be performed. The use of finite element methods to study the stress distribution around ply drops and evaluate static strength has been investigated by numerous authors, including Trethewey et al. (1993), Botting et al. (1996), Mukherjee and Varughese (1999) and Vidyashankar and Krishna Murty (2001). Much of this work took place in the 1990's and a comprehensive review of the ply drop studies conducted during this period is provided by He et al. (2000). More recently, increasing attention has been placed on the analysis of fatigue delamination (Murri, 2006; Murri and Schaff, 2006) but the majority of studies to date have focused on the number of cycles for a crack to initiate at a stress concentration rather than subsequent damage propagation. For structures where fatigue is a critical design driver, such as the tidal turbine blades considered in the current article, considering only crack initiation can lead to over-conservative design, particularly in cases where there are sharp stress concentrations at very localized regions such as ply drops. This is because cracks will tend to initiate at a relatively low proportion of the number of cycles taken for damage to grow to an extent where structural failure becomes a concern, particularly if any manufacturing defects are present. Once a crack has initiated, subsequent crack propagation may either be arrested as the stress redistributes or will be at such a slow rate that the structure can remain safely in service significantly longer than the crack initiation lifetime.

Increased computational processing power and understanding of composite failure has enabled the development of finite element modelling techniques that can simulate damage growth within composite structures. Numerical analysis techniques include the Virtual Crack Closure Technique (Rybicki and Kanninen, 1977; Krueger, 2004) and the use of interface elements, which are specialised finite elements placed along potential failure planes and used to simulate crack growth (Camanho et al., 2003; Jiang et al., 2007; Hallett, 2007). A key advantage of interface elements is that they can encompass both strength based damage initiation criteria and fracture based crack propagation criteria. They can also enable cracks to propagate simultaneously along any interfaces where the interface elements are placed, which is a particular advantage when dealing with very thick laminates containing a range of potential damage paths. Recently, fatigue damage algorithms have been developed and implemented within interface elements to simulate crack growth under cyclic load conditions and these have been applied to predict both composite delamination (Capello and Tumino, 2007; Turon et al., 2007; Harper and Hallett, 2010) and adhesive bond-line failure (Khoramishada et al., 2010).

The use of such methods within the design process offers a far greater understanding of failure than is possible using conventional techniques, which purely predict the number of cycles to failure for a given composite layup sequence and applied fatigue load, and provide no indication of the nature and rate of damage

Published in Ocean Engineering 2015; 96. pp 272–283
DOI: 10.1016/j.oceaneng.2014.12.025

progression prior to final failure. The ability to analyse the nature of damage progression can guide improvements both to the design geometry and composite layup sequence, hence allowing a greater level of design optimisation. It can also allow the impact of potential manufacturing defects, such as unbonded regions between plies, to be analysed, giving greater confidence in the required design safety margins that must be applied and possibly reducing these.

This paper demonstrates how the analysis of interfacial failure using interface elements can aid the structural design of tidal turbine blades using realistic scenarios where cracks can grow simultaneously along several interfacial planes, under both quasi-static and fatigue loading. This extends the authors' previous work (Harper and Hallett, 2010), which gave a first presentation of the numerical method and looked at very basic fracture toughness coupons (DCB, ENF and MMB), where crack growth was only possible along a single plane and occurred under a constant mode-ratio.

In section 2, the main principles of the numerical model are outlined before describing how the model can be integrated with the blade design process to analyse both static strength and fatigue life. Application of the model to a composite ply drop feature typical of that found at the blade root is then demonstrated (sections 3 and 4) to clarify the process and to show how the model can be used to guide design improvements.

2. Methodology

2.1 Principles of Numerical Model

Cohesive interface elements, which are becoming increasingly used for analysing composite delamination and bond-line failure in finite element models, are bespoke elements inserted along potential interfacial failure planes. The interface element incorporates both stress and fracture based failure criteria, enabling both damage initiation and subsequent propagation to be analysed without the need for a pre-crack. Since this paper is intended primarily to demonstrate how the interface element modelling technique can be integrated with the blade design process, only a brief overview of the interface element's numerical formulation is provided and the reader is encouraged to consult Jiang et al. (2007) and Harper and Hallett (2010) for more detailed information on the static and fatigue formulations respectively.

An interface element's behaviour is governed by a traction-displacement curve, in which stress generally increases from zero to the interface material's maximum stress (σ_{max}), before degrading to zero, resulting in complete failure. Although the shape of the interface element traction-displacement curve can take

Published in Ocean Engineering 2015; 96. pp 272–283
DOI: 10.1016/j.oceaneng.2014.12.025

numerous forms, one of the conditions for ensuring an accurate delamination analysis is that the total area enclosed must equal the critical fracture energy of the material (G_C). Figure 3 shows the quasi-static response of a typical interface element formulation, governed by a bi-linear traction-displacement curve, applied to the Double Cantilever Beam (DCB) test for pure mode I (opening) fracture behaviour in composite materials (ASTM D5528-01, 2007). The Global Force-Displacement Response in Figure 3 shows the variation in load (P) at the two cantilever tips as they are subjected to an increasing displacement (Δ). The load initially increases in a linear manner until reaching the critical crack opening displacement (Δ_{crit}), where the strain energy release rate (G) at the crack tip exceeds the fracture toughness of the interface and the crack begins to propagate. The load then decreases as the opening displacement increases further and the crack advances. Figure 3 also shows the corresponding stress and mode I displacement (δ_I) of the initial crack tip interface element before crack propagation occurs. As the cantilever tips start to be displaced, the interface element stress increases linearly with its mode I opening displacement until reaching the maximum interfacial stress (σ_{max}) at its elastic displacement limit (δ_e). This corresponds with point 1 on the global force–displacement curve, which continues to increase linearly at this stage due to adjacent interface elements taking up the additional load. As both the cantilever tip displacement and interface element displacement increase further, the interface element stress linearly decreases as more load is taken up by adjacent interface elements. The rate of this decrease is set to ensure that when stress reaches zero at the failure displacement, and the element can support no load, the area enclosed by the stress-displacement curve is equal to the mode I fracture toughness of the material. The failure displacement (δ_f) corresponds with point 2 on the global force-displacement where the crack begins to advance.

Figure 3: An interface element's traction-displacement response

A similar traction-displacement response exists for pure mode II (shear) fracture behaviour except that the mode I interfacial strength and fracture toughness are replaced by their mode II counterparts. Under the more general case of mixed mode loading, the formulation can be illustrated using a single three-dimensional map by representing the normal opening mode (mode I) on the 0 - σ - δ_{normal} plane, and the transverse shear mode (mode II) on the 0 - σ - δ_{shear} plane, as shown in Figure 4. The triangles 0 - $\sigma_{I,max}$ - $\delta_{I,f}$ and 0 - $\sigma_{II,max}$ - $\delta_{II,f}$ are the bi-linear responses in pure opening mode and in pure shear mode respectively. Any point on the 0 - δ_{normal} - δ_{shear} plane represents a mixed-mode relative displacement.

The mixed mode damage onset displacement, $\delta_{m,e}$, and interfacial strength, $\sigma_{m,max}$, are calculated using a quadratic damage onset criterion:

Published in Ocean Engineering 2015; 96. pp 272–283
DOI: 10.1016/j.oceaneng.2014.12.025

$$\sqrt{\left(\frac{max(\sigma_I,0)}{\sigma_{I,max}}\right)^2+\left(\frac{\sigma_{II}}{\sigma_{II,max}}\right)^2}=1 \qquad \text{(Eqn. 1)}$$

The mixed mode failure displacement corresponding to complete decohesion is calculated using the Benzeggagh-Kenane failure criterion (Benzeggagh and Kenane, 1996):

$$G_C = G_{IC}+\left(G_{IIC}-G_{IC}\right)\left(\frac{G_{II}}{G_T}\right)^{\eta} \qquad \text{(Eqn. 2)}$$

where G_{II} and G_T are the mode II and total (mode I + mode II) crack tip strain energy release rates and G_{IC} and G_{IIC} are fracture toughness values (critical energy release rates) for pure mode I (opening) and pure mode II (shear) respectively. The exponent η is an empirical parameter derived from mixed-mode fracture toughness tests. A value of $\eta=1.12$ has been applied in Equation (2) as this was found to give the best fit to the experimental fracture toughness data for the material analysed in this investigation. Equation (2) allows the locus of complete decohesion, represented by the relative displacement corresponding to complete interface failure, $\delta_{m,f}$, to be determined.

Figure 4: The mixed mode traction-displacement law

The constitutive law for static load cases (Jiang et al., 2007) has recently been extended to enable material degradation and failure under cyclic loading (Harper and Hallett, 2010). The fatigue degradation law is designed to simulate the Paris Law for crack growth, which has become commonly used to characterise both delamination and adhesive bondline failure under fatigue loading. Similar to crack propagation under static loading, the Paris Law relationship characterises crack growth with respect to the crack tip strain energy release rate and can be expressed as:

$$\frac{\partial a}{\partial N}=C\left(\frac{\Delta G}{G_C}\right)^m \qquad \text{(Eqn. 3)}$$

where a is the crack length in the direction of crack growth, N is the number of fatigue cycles and $\partial a/\partial N$ is the crack growth rate per fatigue cycle. ΔG is the change in crack tip strain energy release rate between the maximum and minimum load in each fatigue cycle, G_C is the critical energy release rate, and C and m are constants determined by fitting the curve to experimental data gained from fracture toughness specimens. For linear elastic behaviour, the crack tip strain energy release rate is proportional to the square of the applied load

Published in Ocean Engineering 2015; 96. pp 272–283
DOI: 10.1016/j.oceaneng.2014.12.025

and ΔG can be calculated using the maximum strain energy release rate in each fatigue cycle, combined with the ratio between the minimum and maximum load (P_{min} and P_{max}) in each fatigue cycle, commonly referred to as the R-Ratio ($R=P_{min}/P_{max}$):

$$\Delta G = G_{max} (1 - R^2) \quad \text{(Eqn. 4)}$$

A typical Paris Law Curve is shown in Figure 5 and it is bounded by two key values; the threshold strain energy release rate, ΔG_{th}, below which no crack growth occurs, and the critical fracture energy, G_C, at which a crack will propagate under a static load. G_{max} and G_{min} are the maximum and minimum strain energy release rates within each fatigue cycle.

Figure 5: The Paris Law curve

There is a unique Paris Law curve for each mode-ratio (the ratio between mode I opening and mode II shear loading) and some form of interpolation law is required to determine the Paris Law constants under mixed mode loading. At the time of performing this investigation, no experimental data was available for mixed mode fatigue loading of the relevant material and it was necessary to assume a linear variation of the Paris Law Constants C and m, as proposed by Russell and Street (1989), using Equation (5) and (6) respectively:

$$C = \left(\frac{G_I}{G_T}\right) C_I + \left(\frac{G_{II}}{G_T}\right) C_{II} \quad \text{(Eqn. 5)}$$

$$m = \left(\frac{G_I}{G_T}\right) m_I + \left(\frac{G_{II}}{G_T}\right) m_{II} \quad \text{(Eqn. 6)}$$

where G_I and G_{II} are the mode I and mode II components of the total strain energy release rate, G_T, which are extracted from the numerical model and m_I, C_I, m_{II} and C_{II} are the pure mode I and mode II Paris Law constants gained from experimental data on Double Cantilever Beam (DCB) and End Notch Flexure (ENF) specimens respectively. Figure 6 shows the change in slope of the Paris Law curve applying equations (5) and (6) as mode ratio varies between pure mode I and pure mode II loading.

Figure 6: The Paris Law variation under mixed-mode loading

Recent work at the University of Bristol (Allegri et al., 2013) has developed improved interpolation rules for mixed mode fatigue loading. These will be incorporated into the fatigue interface elements used for the current study in future work.

Published in Ocean Engineering 2015; 96. pp 272–283
DOI: 10.1016/j.oceaneng.2014.12.025

All of the analyses presented in this paper were performed using the explicit Finite Element code LS-Dyna. In order to simulate cyclic loading within the model, it is not numerically feasible to explicitly vary the applied load for the hundreds of thousands of cycles that the turbine blade will experience during its lifetime. Instead, a loading envelope strategy is employed, where the component being modelled is initially loaded to the maximum load in each fatigue cycle. Having allowed enough time for any dynamic effects to stabilise, the fatigue degradation law is then activated and although the load applied in the finite element load remains at the maximum in each fatigue cycle, the law allows the interface to weaken on the assumption that it is being subjected to continuous fatigue loading. The fatigue law itself performs the following main functions in order to allow this process to occur:

1. Extraction of the mode I and mode II strain energy release rate from interface elements within the model.

2. Calculation of the required rate of crack growth using the Paris Law model (Equations (3) to (6)).

3. Application of an interface element strength degradation law, causing them to fail at a rate which reproduces the required rate of crack advance provided by the Paris Law model.

These functions are illustrated in Figure 7 using the example of a composite ply drop, a design feature which is studied in detail in subsequent sections of this paper.

Figure 7: Functions of the numerical model

2.2 Application to Blade Design Process

Due to the small finite element size needed to accurately simulate crack growth within specific layers of a laminate, it would be too computationally demanding to apply this modelling process to the entire turbine blade structure. Therefore, it is first necessary to identify regions of the blade where high stress concentrations occur and hence, which are most susceptible to failure under both extreme one-off load cases and fatigue loading. This can be achieved using relatively simple structural models of the blade, where only the main profiles of components such as spars and ribs are considered and material properties are assumed to be constant through the thickness of each component (i.e. detailed design features such as ply drops, holes, cut-outs, bonded joints and the precise composite ply layup sequence within each component are not considered at this stage). Detailed finite element models can now be produced of the most highly stressed regions, where composite plies are modelled as discrete layers with material properties assigned according to the fibre direction within each layer. Interface elements are inserted between the composite plies and along any adhesive bond-lines present to enable

interfacial failure. Potential manufacturing defects, in the form of embedded delaminations, can also be modelled by excluding interface elements at locations where they are likely to have the most detrimental impact on structural integrity. These more detailed models can be analysed to determine whether the structural features can withstand both static and fatigue design load cases.

Under fatigue loading, the models can be used to apply a damage tolerant design approach, where some crack growth from stress concentrations is allowed provided this does not compromise the blade's structural integrity. Such an approach offers the potential for a reduction in design safety margins relative to a conventional 'no growth' design philosophy, where stresses must remain below levels at which crack onset occurs. The model can be used to analyse the number of fatigue cycles to failure for a given applied fatigue load or the residual strength after a specified number of cycles. This can be done for any potential sequence of ply fibre orientations and sensitivity analyses can be conducted to evaluate the impact of design uncertainties, such as the size/location of manufacturing defects and geometrical tolerances.

The ability to explicitly model damage progression in this manner can reduce the physical test requirement by enabling design optimization to be done with the numerical models, before progressing to more expensive and time consuming validation tests on structural components. Coupled with improved understanding of potential failure mechanisms and damage growth rates, this can ultimately lead to improved design and reduced safety margins, enabling a reduction in the mass of material required for blade manufacture. A leaner blade structure enables the external profile to more closely match the ideal hydrodynamic design for maximum energy extraction, particularly in the highly stressed root region, where the need for very thick composite sections currently limits this. Hence, the tidal stream energy device can be made more cost-effective through two main avenues; a direct material cost saving and improved energy extraction from the device over its required lifetime.

3. Model Setup and Input Parameters

The potential application of these analysis techniques within the design process can be explored through a study on composite ply drops, which are used to gradually reduce the thickness of material along the length of the blade. The ply drop geometries used in this investigation are based on those from a recent study that used the Virtual Crack Closure Technique, rather than cohesive interface elements, to analyse delamination (Giannis, 2013).

Published in Ocean Engineering 2015; 96. pp 272–283
DOI: 10.1016/j.oceaneng.2014.12.025

The most basic case of an external ply drop specimen (see Figure 8) with uni-directional plies (fibres running parallel to specimen length) is initially investigated, as a simplified validation case for the models. Results for a more complex case of a cover ply specimen (Figure 9) with multiple ply orientations, where failure involves simultaneous crack growth along several interfacial planes are then discussed. All of these investigations are performed under both a quasi-static tensile load until failure and at various tensile fatigue load levels with an R-Ratio of 0.1 until failure.

Figure 8: External ply prop specimen

Figure 9: Cover ply specimen

It is assumed that the ply drop is part of the blade's spar cap, where carbon-fibre would be used for manufacture due to the high strength and stiffness requirement of this component.

The material properties used are for High Strength Carbon/Epoxy pre-preg, as shown in Table 1 (Aviation Enterprises Ltd material MRC044), and were provided by Element Hitchin Ltd, a specialist material testing laboratory. Element Hitchin Ltd also provided all experimental data subsequently presented for the ply drop specimen tests, allowing comparison with the numerical modelling results. The pre-preg had an areal weight of 600g/m^2, which resulted in a cured ply thicknesses of 0.65mm. This material is commonly used for the manufacture of thick composite laminates for marine renewable energy applications such as tidal turbine blade spar caps, where a high load bearing capability is required.

Table 1: Laminate and Interfacial Properties

Laminate Properties		**Interfacial Properties (applied to interface elements)**			
		Static Properties		**Fatigue Properties**	
E_{11} (MPa)	110,500	G_{IC} (N/mm)	0.21, 0.85	C_I (N/mm)	2.84×10^{-2}
$E_{22} = E_{33}$ (MPa)	7,825	G_{IIC} (N/mm)	1.15	C_{II} (N/mm)	1.21×10^{-1}
$G_{12} = G_{13}$ (MPa)	3900	$\sigma_{I,max}$ (MPa)	45	m_I	4.52
G_{23} (MPa)	1985	$\sigma_{II,max}$ (MPa)	75	m_{II}	3.69
$v_{12} = v_{13}$	0.36	K_I (N/mm^3)	100,000		
v_{23}	0.4	K_{II} (N/mm^3)	100,000		

Published in Ocean Engineering 2015; 96. pp 272–283
DOI: 10.1016/j.oceaneng.2014.12.025

For the cover ply model, the resin pocket was modelled as an isotropic elastic material with a modulus of 2760 MPa and poisson ratio of 0.35.

With respect to the interfacial properties, two separate values of G_{IC} were used for the modelling work conducted to investigate the effects of crack bridging, a process whereby intact fibres bridge the two surfaces of a growing crack and act to resist further growth. The lower value of 0.2125 N/mm occurs at crack propagation onset, before any crack bridging develops, and the higher value of 0.85 N/mm occurs once a significant amount of crack bridging has developed behind the growing crack front. Both of these values were determined by DCB fracture toughness tests on uni-directional specimens and a graphical representation of the increase in fracture toughness observed in these tests is shown in Figure 10, courtesy of Element Hitchin Ltd.

Figure 10: Variation in G_{IC} with delamination length

For the interfacial strengths, $\sigma_{I,max}$ and $\sigma_{II,max}$, no experimental data was available. Therefore, based on previous interface element modelling work performed at the University of Bristol, values of $\sigma_{I,max}$ = 45 MPa and $\sigma_{II,max}$ = 75 MPa were applied. The interfacial parameters K_I and K_{II} in Table 1 are the interface element stiffness prior to damage initiation (i.e. the elastic region of the traction-displacement curve) under pure mode I and pure mode II loading respectively. K_I and K_{II} are not experimentally determined but satisfy the requirements of providing a high stiffness interface without exceeding a value that would lead to numerical instabilities. All numerical modelling work was conducted using the explicit Finite Element code, LS-Dyna, and results are compared with experimental data for equivalent ply drop specimens.

4. Results

4.1 External Ply Drop

For quasi-static loading, Figure 11 shows how interfacial damage in the uni-directional external ply drop specimen progresses under increasing tensile stress in the core laminate, with G_{IC} at its lower value of 0.2125 N/mm. Crack onset between the core and final zero degree ply drop occurs at approximately 570 MPa, with unstable delamination occurring shortly afterwards at 595 MPa. In the experimental tests, the mean visual crack initiation stress of 513 MPa showed reasonable agreement with the numerical results, but final failure occurred at a far greater mean stress of 675 MPa. It is believed that this was due to the effects of crack bridging as the crack propagates, which causes a rise in G_{IC}. Using the higher value of G_{IC} = 0.85 N/mm, unstable delamination occurred at a stress of 715 MPa, showing a closer match to the experimental final failure stress, as

Published in Ocean Engineering 2015; 96. pp 272–283
DOI: 10.1016/j.oceaneng.2014.12.025

shown in Figure 12. These results suggest that future models should incorporate a varying G_{IC} value in interface elements, with a lower value not including the effects of crack bridging in regions of crack initiation and a higher value to account for crack bridging away from these locations.

Figure 11: Damage progression in the uni-directional external ply drop specimen with G_{IC} = 0.21 N/mm

Figure 12: Comparison of experimental crack initiation and final failure stress against numerical failure stress with G_{IC} = 0.21 N/mm and G_{IC} = 0.85 N/mm

For fatigue loading, numerical analyses were again performed using the high and low values of fracture toughness. These were plotted against two experimental data sets:

i) The number of cycles for a crack to initiate (measured by observation in the experimental tests) and propagate 5 mm along the interface between the cover ply and final ply drop, referred to as 'total life.'
ii) The number of cycles for a crack to propagate 5 mm along the interface between the cover ply and final ply drop following crack initiation, referred to as 'propagation life'.

In Figure **13**, the numerical and experimental fatigue lives are plotted against the maximum axial stress in the core laminate in each fatigue cycle. Due to the differences in the absolute values between numerical and experimental results in the static case as noted in figure 12, fatigue results are presented normalised against the relevant numerical static value. Raising G_{IC} in the numerical simulations is seen to significantly reduce the rate of crack propagation for a given fatigue load, which is consistent with the increased static failure stress at a higher G_{IC} value. The experimental fatigue data appears to give closer correlation with numerical results for G_{IC} = 0.21 N/mm at low fatigue loads and for G_{IC} = 0.85 N/mm at high fatigue loads. This suggests that the fatigue load level may be influencing the damage mechanisms around the crack tip and the resultant amount of crack bridging as the crack propagates, but this requires further investigation in future work. The experimental results for total life and propagation life exhibit close correlation, indicating that fatigue life is dominated by the crack propagation stage, even for this relatively small crack length failure criterion of 5 mm. The experimental results exhibit good correlation with the numerical results at high fatigue load levels, but shorter than predicted fatigue lives at low fatigue load levels.

Figure 13**: External ply drop fatigue lives against normalised load level**

4.2 Single Cover Ply Results

Published in Ocean Engineering 2015; 96. pp 272–283
DOI: 10.1016/j.oceaneng.2014.12.025

Figure 14 shows the damage progression sequence for the single cover ply specimen with G_{IC} = 0.21 N/mm under quasi-static loading. Due to the high mode I load component where the cover ply falls onto each internal ply, significant delamination between the cover ply and internal plies occurs at stresses far below the final failure stress. Initial crack propagation between the cover ply and step 4 occurs at 28% of the final failure load. This initial propagation is stable and progresses to a length of about 5 mm before a delamination initiates at the next cover ply/internal ply drop interface. Delaminations between the cover ply and internal plies continue to grow in a stable manner until final failure occurs, which is via an unstable delamination along the interface between step 1 and step 2. Crack propagation begins along this interface at an axial stress in the core laminate of 980 MPa and rapidly becomes unstable, causing complete specimen failure at 1080 MPa. Figure 15 shows this sequence of damage events on a stress-displacement chart, where the experimental results, courtesy of Element Hitchin Ltd, and results for the external ply drop model are also shown for comparison. Final failure in the experimental test specimens occurred at a 25% greater failure stress of 1352 MPa and the damage progression sequence showed the following differences compared with the numerical model:

i) Damage initiation in experiments was observed at a mean tensile stress of 975 MPa at the end of the terminating 0 degree ply (step 2 in figure 14) and a crack was seen to propagate simultaneously towards both the thick and thin end of the specimen (along the 0 degree/-45 degree interface and the cover ply/-45 degree interface). Although this shows close agreement with the numerical model with respect to initial crack propagation between the 0 degree/-45 degree interface, which occurred at 980 MPa, it shows poor agreement with initial crack propagation between the cover ply/-45 degree interface, which occurred at 300 MPa in the models. This requires further investigation but may be partly attributable to the insertion of a small 0.2 mm void at the end of the resin pocket in the numerical model, which was not present in the experimental specimens. It could also be due to different interfacial properties (e.g. higher fracture toughness) occurring between the resin pocket and cover ply to those measured in the fracture toughness specimens and applied uniformly in the numerical model.

ii) In the experimental specimens, interfacial cracks were observed to jump through the -45 degree ply and interfacial crack propagation also occurred between the core and the -45 degree ply, both towards the thin and thick end of the specimen. Future numerical models will need to include interface elements within the -45 degree ply to allow these effects to be simulated.

Figure 14**:Interfacial damage progression in the cover ply specimen with G_{IC} = 0.21 N/mm**

Published in Ocean Engineering 2015; 96. pp 272–283
DOI: 10.1016/j.oceaneng.2014.12.025

Figure 15**: Numerical stress-displacement curve for the cover ply specimen with G_{IC} = 0.21 N/mm**

The effect of a 1 mm manufacturing defect at the end of each ply drop termination was also investigated for the cover ply specimen, which would be typical of a defect in a real blade caused by a thin segment of release film remaining attached to the end of a ply. This was achieved by deleting a 1 mm strip of interface elements in the numerical models and by inserting a starter crack in the experimental specimens using release film. Other defect types were outside of the scope of this piece of work, but such high-fidelity modelling techniques are the subject of ongoing work at the University of Bristol (Mukhopadhyay et al., 2013; Li et al., 2013). Further investigation of potential manufacturing defects in tidal turbine blade structures and their effects on damage progression and failure will be important in future studies.

The 1mm defect was found to have no significant impact on either the damage progression sequence or final failure load in the numerical model and this was consistent with the experimental results, where the mean failure load for specimens with defects was recorded as 1362 MPa, compared to 1352 MPa without defects.

Due to the large amount of cover ply delamination occurring in the numerical analyses prior to final failure, which was not observed experimentally, the effect of raising G_{IC} to 0.85 N/mm was again investigated. This had little effect on the final failure load, since it is governed by the mode II dominated interfacial failure between step 1 and step 2, however it did significantly increase both the cover ply delamination onset loads and the extent of cover ply delamination prior to final failure. The damage progression sequence with G_{IC} = 0.85 N/mm and defects included is shown in Figure 16.

Figure 16: Interfacial damage progression in the Single Cover Ply Specimen with G_{IC} = 0.85 N/mm (1 mm defects included)

Figure 17 shows fatigue results for the cover ply specimen using the normalised fatigue load level. All fatigue analyses were conducted with 1 mm defects inserted for consistency with the experimental tests. A G_{IC} value of 0.85 N/mm was applied throughout because initial trials with the lower value of 0.2125 N/mm gave extremely short fatigue lives due to large cover ply delaminations, which were unrepresentative of the experimental tests. The nature of damage progression was similar to that for the static analyses, with the critical delamination growing between the step 1/step 2 interface. In this case, fatigue life was defined as the number of cycles for the critical delamination to reach a length of 20 mm, rather than 5 mm, as previously used for the external ply drop specimen. This was due to the large initial crack growth rate, which resulted in very low

Published in Ocean Engineering 2015; 96. pp 272–283
DOI: 10.1016/j.oceaneng.2014.12.025

fatigue lives when using a length of only 5 mm. Similar to the external ply drop specimen, the total experimental fatigue life was dominated by the crack propagation phase (i.e. cracks were generally seen to initiate at a low number of fatigue cycles relative to the total number of cycles for a crack to propagate 20 mm). Similar to the external ply drop specimen, a reasonable level of correlation was gained between the experimental and numerical results.

Figure 17: Cover ply specimen fatigue lives against normalised load level

5. Conclusions and Future Work

The ability to model interfacial damage progression in the structural features of tidal turbine blades has potential to aid blade design optimisation and reduce the physical test requirement in the design process. In the current study, this has been demonstrated using ply drop features, which are used to taper the thickness of material along the length of primary load bearing structures such as blade spars. Numerical analyses of the ply drops have shown a promising level of correlation with experimental test results for both static and fatigue load cases, with input parameters for the models obtained purely from small-scale coupon tests (e.g. fracture toughness specimens such as the DCB and ENF). Some further work is still needed to refine their accuracy in terms of absolute values predicted.

The static and fatigue analyses conducted on the external ply drop specimen have shown the importance of developing an ability to vary interfacial fracture toughness as a crack progresses, to account for crack bridging effects and more accurately simulate crack propagation. This can potentially be achieved by varying the G_{IC} value in interface elements, with a lower value not including the effects of crack bridging in regions of crack initiation and a higher value to account for crack bridging away from these locations. In the case of the cover ply model, further work is required to better understand the factors influencing the mode I dominated cover ply delaminations occurring prior to final failure and why these were less significant in the experimental tests. Particular attention should be placed on investigating the effects of the interfacial properties applied to the resin pocket and how geometric details such as voids influence the results. For models with +/-45 degree plies, there is also a need to investigate how crack branching through the thickness of individual plies can be modelled, possibly by inserting interface elements through the thickness of plies at critical locations.

Further improvement to the current Paris Law fatigue model may be possible if mixed mode fatigue data becomes available from fracture toughness specimens. This will allow the accuracy of the current linear

interpolation law to be evaluated and if necessary, an improved interpolation law can be implemented to better match experimental results. For the cases studied in this paper, fatigue damage progression was dominated by the crack propagation phase and was therefore compatible with the Paris Law modelling approach applied, which can only account for the propagation stage of fatigue life. Combining the Paris Law modelling approach with a separate analysis technique to predict crack initiation lifetime may be necessary to improve future modelling results and avoid the risk of over-conservative design.

5. Acknowledgements

The authors would like to express their thanks to the support of their industrial partners in conducting these studies; Cytec for supplying composite materials, Aviation Enterprises Ltd for manufacturing test specimens and Element Hitchin Ltd for supplying the experimental results against which the numerical model results have been compared. Work was co-funded by the Technology Strategy Board's Collaborative Research and Development programme, following an open competition. The Technology Strategy Board is an executive body established by the Government to drive innovation. It promotes and invests in research, development and the exploitation of science, technology and new ideas for the benefit of business - increasing sustainable economic growth in the UK and improving quality of life (www.innovateuk.org).

Published in Ocean Engineering 2015; 96. pp 272–283
DOI: 10.1016/j.oceaneng.2014.12.025

References

Allegri, G., Wisnom, M.R., Hallett, S.R., 2013. A New Semi-Empirical Law for Variable Stress-Ratio and Mixed-Mode Fatigue Delamination Growth. Composites Part A. 48, 192-200.

ASTM D5528-01(2007)e1. Standard Test Method for Mode I Interlaminar Fracture Toughness of Unidirectional Fiber-Reinforced Polymer Matrix Composites.

Benzeggagh, M.L., Kenane, M., 1996. Measurement of mixed-mode delamination fracture toughness of unidirectional glass/epoxy composites with mixed-mode bending apparatus. Compos. Sci. Technol. 56, 439-449.

Black & Veatch Consulting Ltd., 2011. UK Tidal Current Resource & Economics, Project Number 121393, Carbon Trust, London.

Bossanyi, E.A., 2007. GH Tidal Bladed Theory Manual, GH & Partners Ltd.

Botting, A.D., Vizzini, A.J., Lee, S.W., 1996. Effect of ply-drop configuration on delamination strength of tapered composite structures. AIAA J. 34, 1650-1656.

Camanho, P.P., Dávila, C.G., de Moura, M.F., 2003. Numerical simulation of mixed-mode progressive delamination in composite materials. J. Compos. Mater. 37 (16), 1415–1438**.**

Charlier, R.H., 2003. A "sleeper" awakes: tidal current power. Renew. Sust. Energ. Rev. 7, 515-529**.**

Davies, P., Germain, G., Gaurier, B., Boisseau, A., Perreux, D., 2013. Evaluation of the durability of composite tidal turbine blades. Philos. T. Roy. Soc. A. 371 (1985).

Boisseau, A., Davies, P., Thiebaud, F., 2013. Fatigue behaviour of glass fibre reinforced composites for ocean energy conversion systems. Appl. Compos. Mat. 20 (2), 145-155.

Droniou, E., Norris, J.V., 2007. Update on EMEC activities, resource description, and characterisation of wave-induced velocities in a tidal flow, Proceedings of the 7th European Wave and Tidal Energy Conference, Porto, Portugal, 2007

Det Norske Veritas AS (DNV), 2008. Certification of Tidal & Wave Energy Converters. Offshore Service Specification DNV-OSS-312.

Fraenkel, P., 2004. Windmills below the sea: A commercial reality soon? Refocus. 5 (2), 46-48.

Gant, S., Stallard, T., 2008. Modelling a Tidal Turbine in Unsteady Flow, Proceedings of the Eighteenth International Offshore and Polar Engineering Conference, Vancouver, BC, Canada, July 6-11, 2008.

Germanischer Lloyd (GL), 2005. Rules and Guidelines, IV – Industrial Services, Guideline for the Certification of Ocean Energy Converters, Part 1: Ocean Current Turbines.

Giannis, S., 2013. Utilising fracture mechanics principles for predicting the mixed-mode delamination onset and growth in tapered composite laminates. Compos. Struct. 102, 294-305

Hallett, S. R., 2008. Predicting progressive delamination via interface elements, in: Sridharan, S. (Ed.), Delamination Behaviour of Composites. Woodhead Publishing Ltd, Cambridge.

Harper, P.W., Hallett, S.R., 2010. A fatigue degradation for cohesive interface elements – Development and application to composite materials. Int. J. Fatigue. 32 (11), 1774-1787.

Harris, B. (Ed.), 2003. Fatigue in Composites. Woodhead Publishing Ltd, Cambridge.

He, K., Hoa, S.V., Ganesan, R., 2000. The study of tapered laminated composite structures: a review. Compos. Sci. Technol. 60, 2643-2657.

Jiang, W,G,. Hallett, S.R., Green, B.G., Wisnom, M.R., 2007. A concise interface constitutive law for analysis of delamination and splitting in composite materials and its application to scaled notched tensile specimens. Int. J. Numer. Methods Eng. 69, 1982-1995.

Jones, R.M., 1999. Mechanics of composite materials, second ed. Taylor and Francis, London.

Jonkman, B.J., Kelley, N.D., 2007. Overview of the TurbSim Stochastic Inflow Turbulence Simulator, Version 1.21 (Revised February 1, 2007), Technical Report NREL/TP-500-41137.

H. Khoramishada, A.D. Crocombe, K.B. Katnama, I.A. Ashcroft, 2010. Predicting fatigue damage in adhesively bonded joints using a cohesive zone model. Int. J. Fatigue. 32, 1146-1158.

Krueger, R., 2004. Virtual Crack Closure Technique: History, approach and applications. Appl. Mech. Rev. 57 (2), 109-118.

Lawrence, J., Kofoed-Hansen, H., Chevalier, C., 2009. High-resolution Metocean modelling at EMEC's (UK) Marine Energy Test Sites. Proceedings of the 8th European Wave and Tidal Energy Conference, Uppsala, Sweden, 2009.

Li, X., Hallett, S.R., Wisnom, M.R., 2013. Modelling the effect of Gaps and Overlaps in Automated Fibre Placement (AFP) manufactured laminates. 19th International Conference on Composite Materials (ICCM 19), Montreal.

Marsh, G., 2004. Tidal Turbines Harness the Power of the Sea. Reinforced Plastics. 48 (6), 44-47.

McCann, G., 2007. Tidal current turbine fatigue loading sensitivity to waves and turbulence – a parametric study. Proceedings of the 7th European Wave and Tidal Energy Conference, Porto, Portugal, 2007.

McCann, G., Thomson, M., Hitchcock, S., 2008. Implications of Site Specific Conditions on the Prediction of Loading and Power Performance of a Tidal Stream Device. 2nd International Conference on Ocean Energy (ICOE), 15th – 17th October 2008, Brest, France.

McGowan, J.G., Hyers, R.W., Sullivan, K.L., Manwell, J.F., Nair, S.V., McNiff, B., Syrett, B.C., 2007. A review of materials degradation in utility scale wind turbines. Energy Materials. 2 (1), 41-64.

Mukherjee, A., Varughese, B., 1999. Development of a specialised finite element for the analysis of composite structures with ply drop-off. Compos. Struct. 46, 1-16.

Mukhopadhyay, S., Jones, M.I., Hallett, S.R., 2013. Modelling of out-of-plane fibre waviness; tension and compression tests. IV ECCOMAS Thematic Conference on the Mechanical Response of Composites (Composites 2013), Ponta Delgada.

Murri, G.B., 2006. Testing and life prediction for composite rotor hub flexbeams. Int. J. Fatigue. 28, 1124-1135.

Murri, G.B., Schaff, J.R., 2006. Fatigue life methodology for tapered hybrid composite flexbeams. Compos. Sci. Technol. 66, 499-508.

RenewableUK, 2012. Marine Energy in the UK: State of the Industry Report 2012.

Russell, A.J., Street, K.N., 1989. Predicting Interlaminar Fatigue Crack Growth rates in Compressively Loaded Laminates. Composite Materials: Fatigue and Fracture, Second Volume, ASTM STP 1012, Paul A. Lagace, Ed., American Society for Testing and Materials, Philadelphia, 1989, pp. 162-178.

Rybicki, E.F., Kanninen, M.F., 1977. A finite element calculation of stress intensity factors by a modified crack closure integral. Eng. Fract. Mech. 9, 931-938.

Sutherland, H.J., 1999. On the Fatigue Analysis of Wind Turbines. Sandia National Laboratories, SAND99-0089.

Sutherland, H.J., Mandell, J.F., 2004. The Effect of Mean Stress on the Damage of Wind Turbine Blades, J. Sol. Energ. – T. ASME. 126, 1041-1049.

Technology Strategy Board (TSB) Press Release, 11th August 2008, http://www.innovateuk.org/content/news/10m-investment-in-new-materials-technologies-to-he.ashx (Accessed 29/12/13)

Trethewey B. R., Gillespie J. W., Wilkins D. J., 1993. Delamination in Thickness Tapered Composite Laminates. J. Eng. Mater. Technol. 115, 193-199

Tumino, D., Cappello, F., 2007. Simulation of Fatigue Delamination Growth in Composites with Different Mode Mixtures. J. Compos. Mater. 41, 2415-2441.

Turon, A., Costa, J., Camanho, P.P., Davila, C.G., 2007. Simulation of delamination in composites under high-cycle fatigue. Composites Part A. 38, 2270-2282.

Vidyashankar, B.R., Krishna Murty, A.V., 2001. Analysis of laminates with ply drops. Compos. Sci. Technol. 61, 749-758.

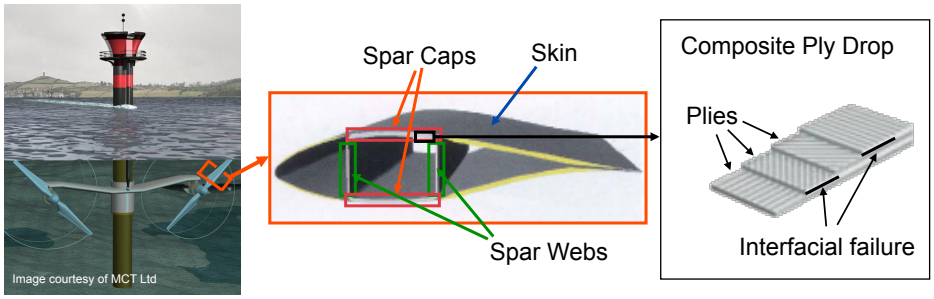

Figure 1: A typical tidal turbine blade structure

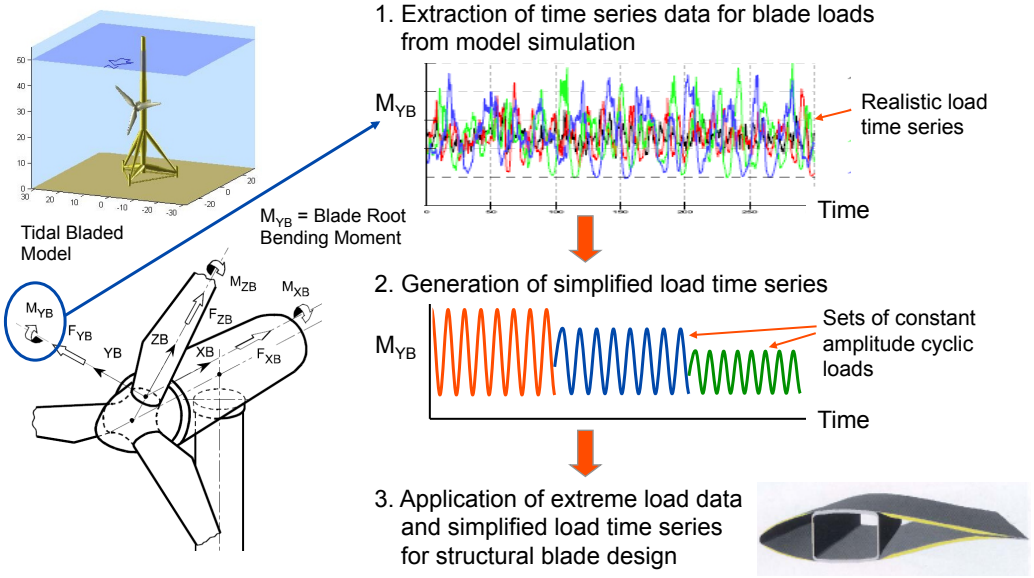

Figure 2: The Structural Design Process for Tidal Turbine Blades

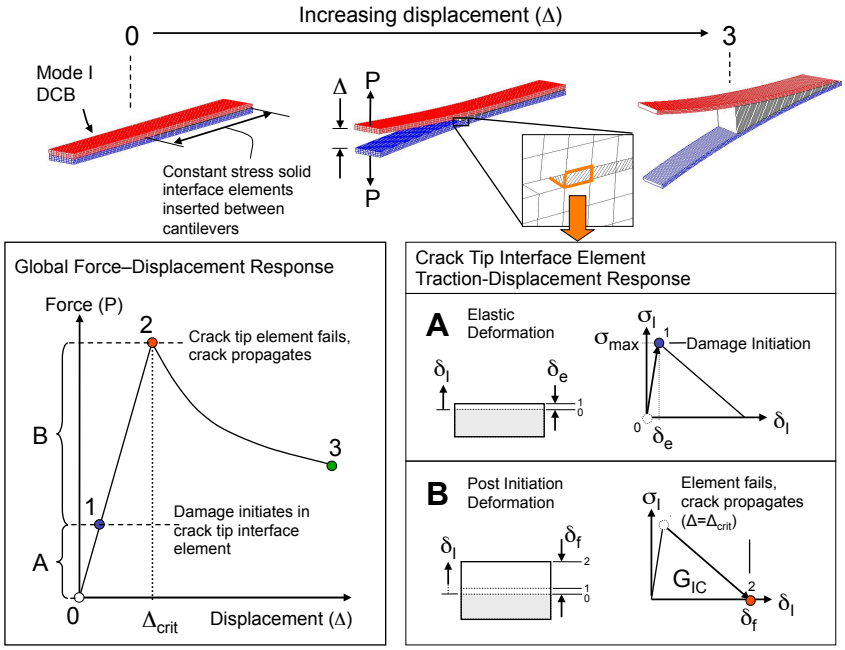

Figure 3: An interface element's traction-displacement response

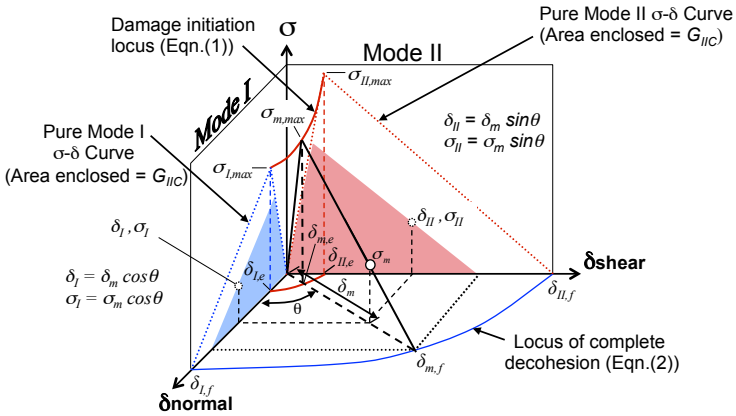

Figure 4: The mixed-mode traction-displacement law

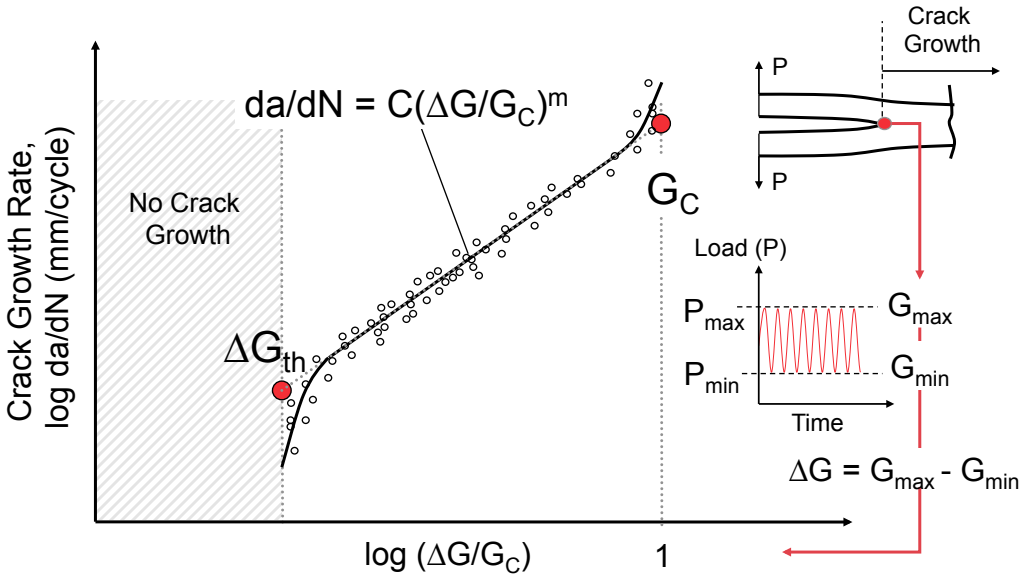

Figure 5: The Paris Law curve

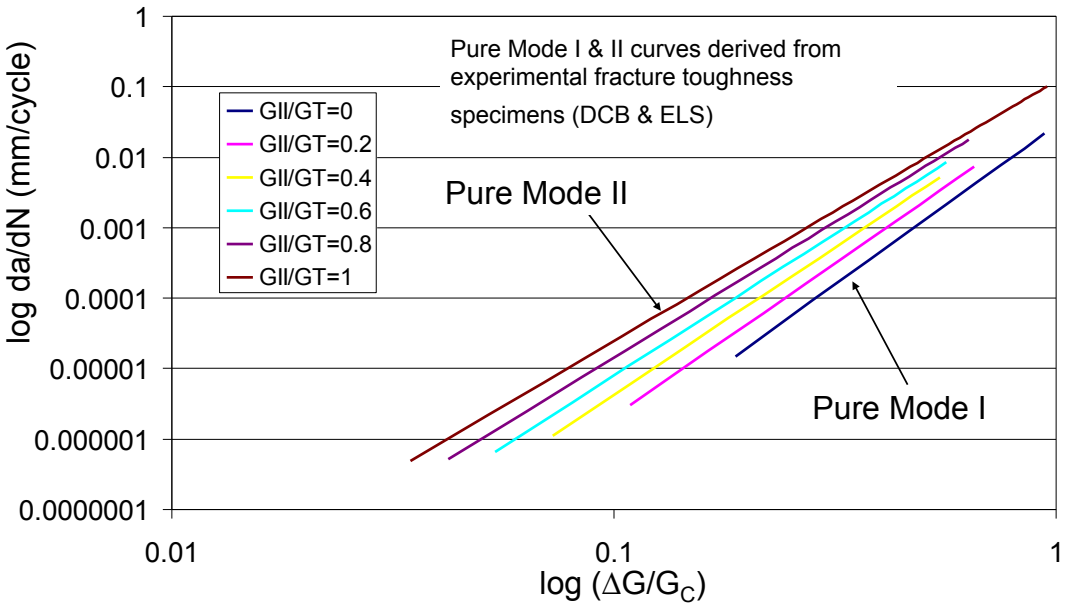

Figure 6: The Paris Law variation under mixed mode loading

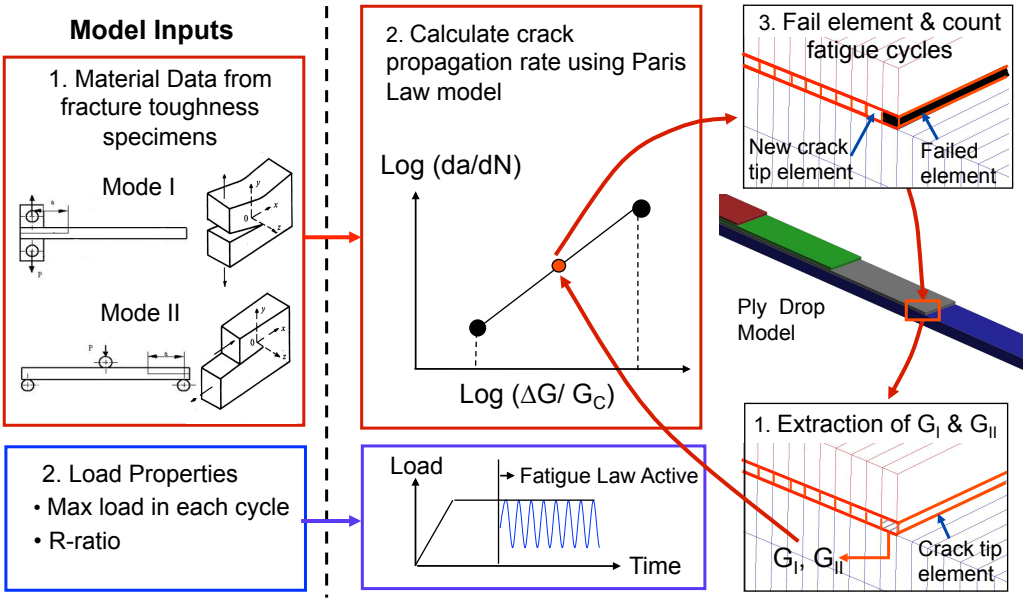

Figure 7: Functions of the numerical model

¼ model used for all analyses

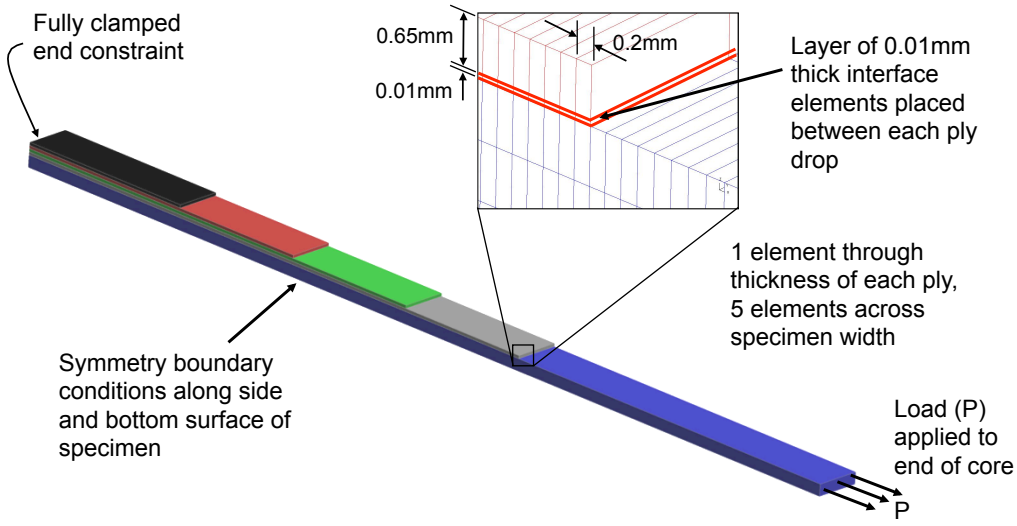

Figure 8: External ply drop specimen

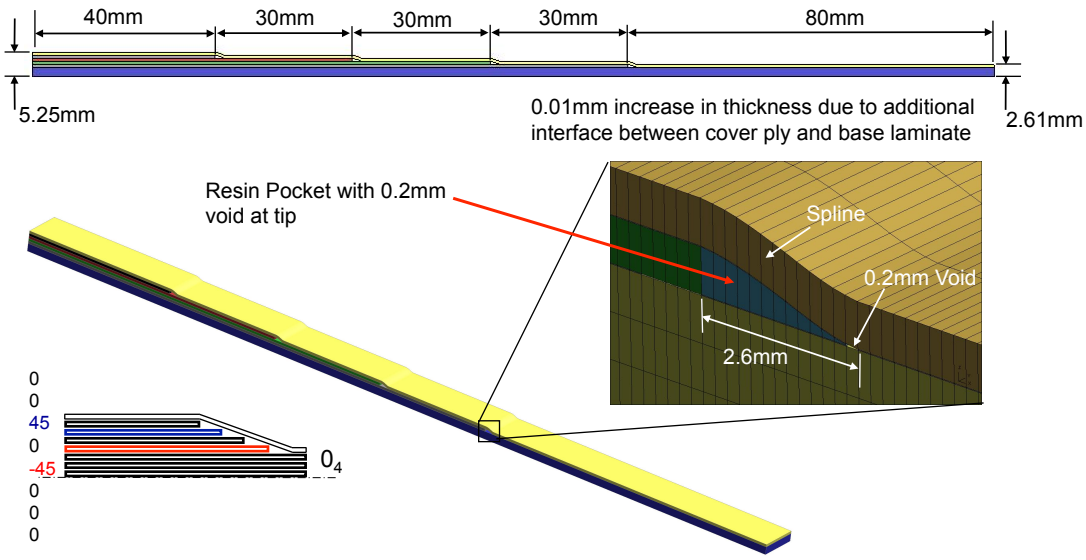

Figure 9: Cover ply specimen

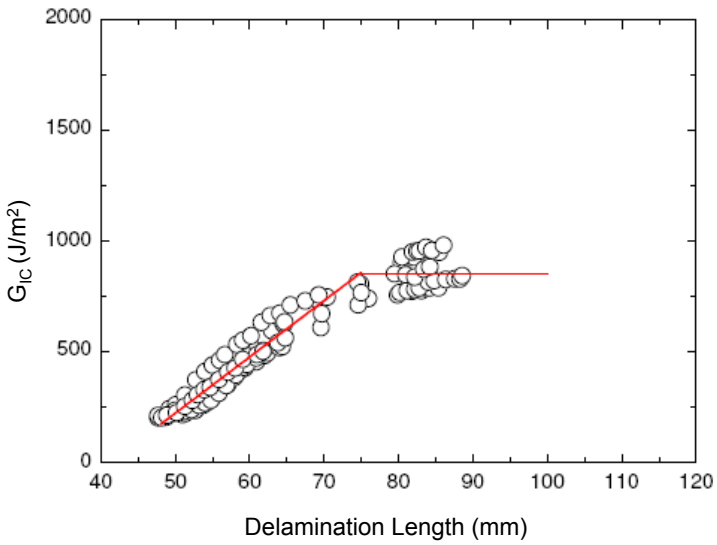

Figure 10: Variation in GIC with delamination length

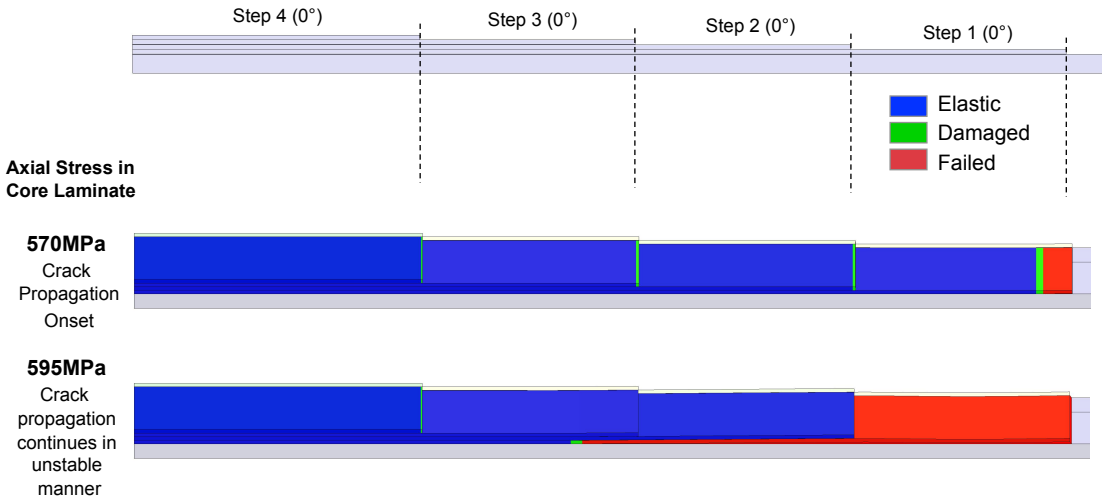

Figure 11: Damage progression in the uni-directional external ply drop specimen with G_{IC} = 0.21 N/mm

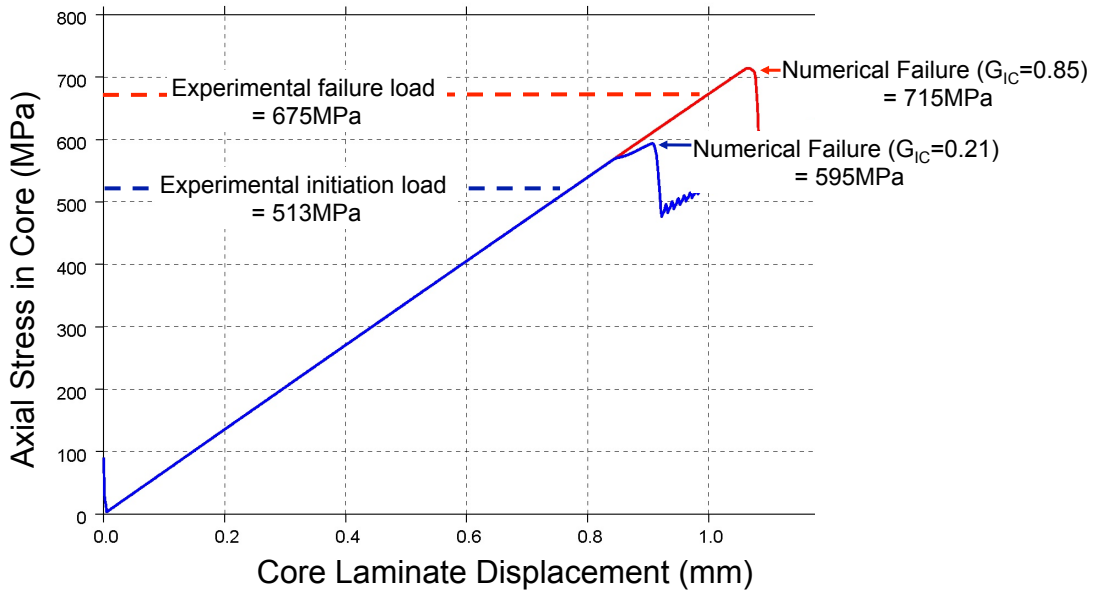

Figure 12: Comparison of experimental crack initiation and final failure stress against numerical failure stress with G_{IC} = 0.21 N/mm and G_{IC} = 0.85 N/mm

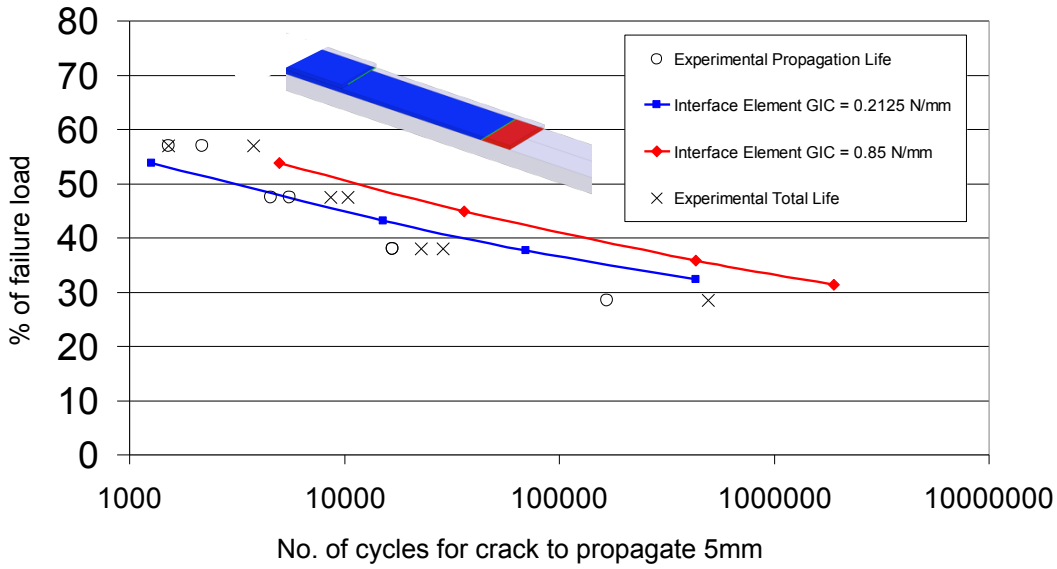

Figure 13: External ply drop fatigue lives against normalised load level

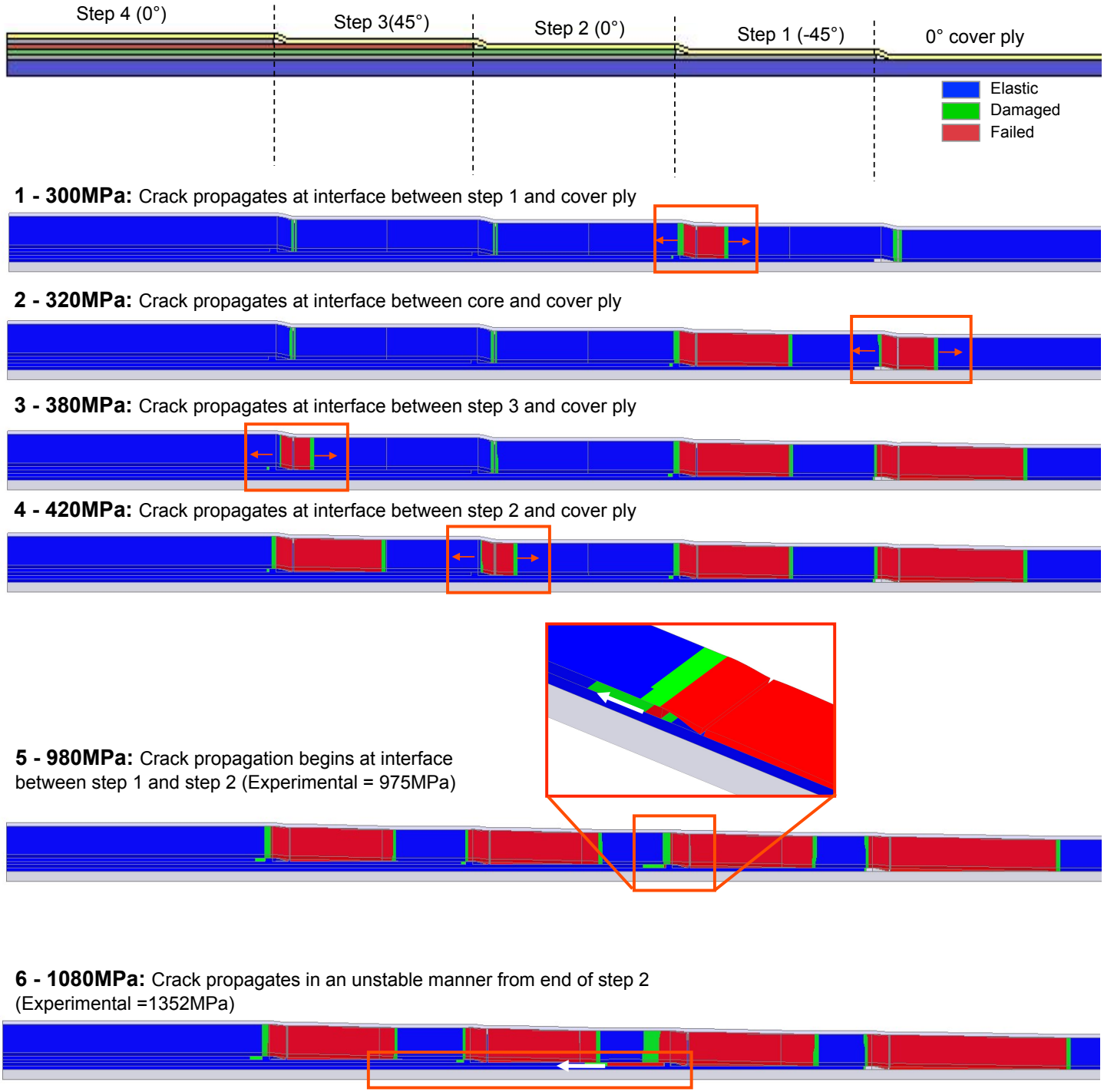

Figure 14: Interfacial damage progression in the cover ply specimen with G_{IC} = 0.21 N/mm (no defects)

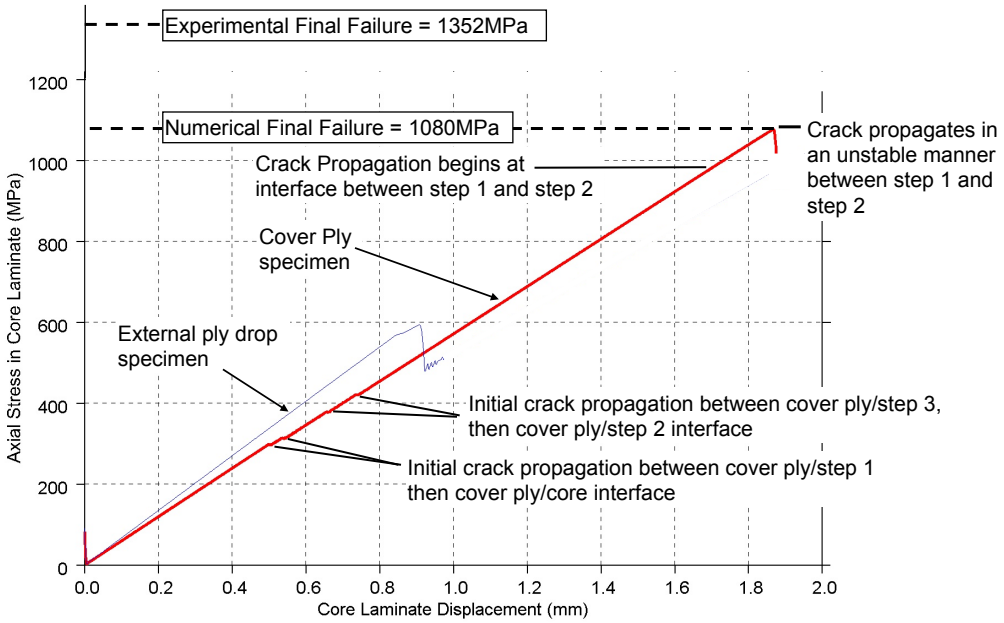

Figure 15: Numerical stress-displacement curve for the cover ply specimen with G_{IC} = 0.21 N/mm

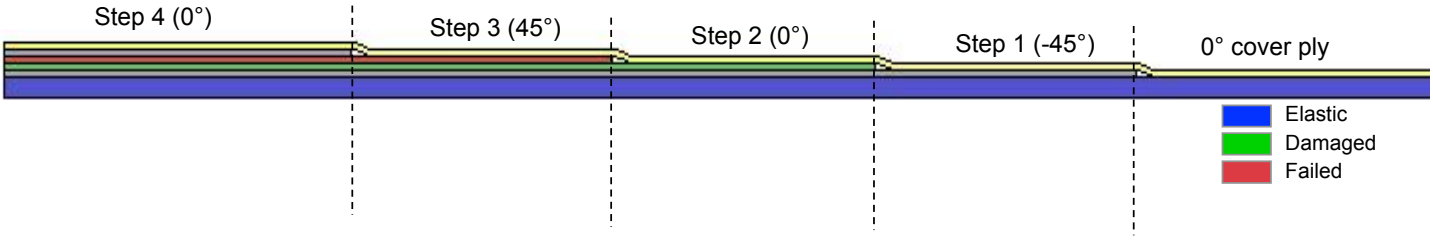

2 - 490MPa: Crack propagates at interface between step 1 and cover ply

3 - 500MPa: Crack propagates at interface between core and cover ply

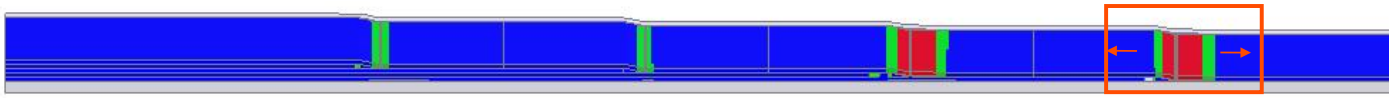

4 - 610MPa: Crack propagates at interface between step 3 and cover ply

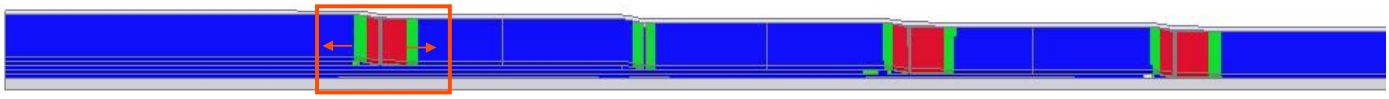

5 - 640MPa: Crack propagates at interface between step 2 and cover ply

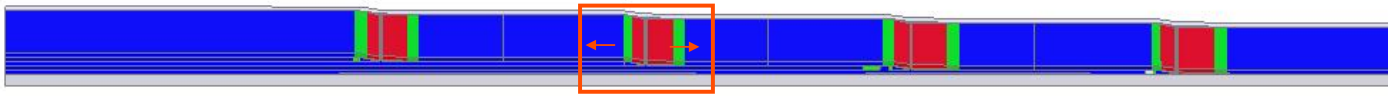

6 - 920MPa: Crack propagation begins at interface between step 1 and step 2 (Experimental = 861MPa)

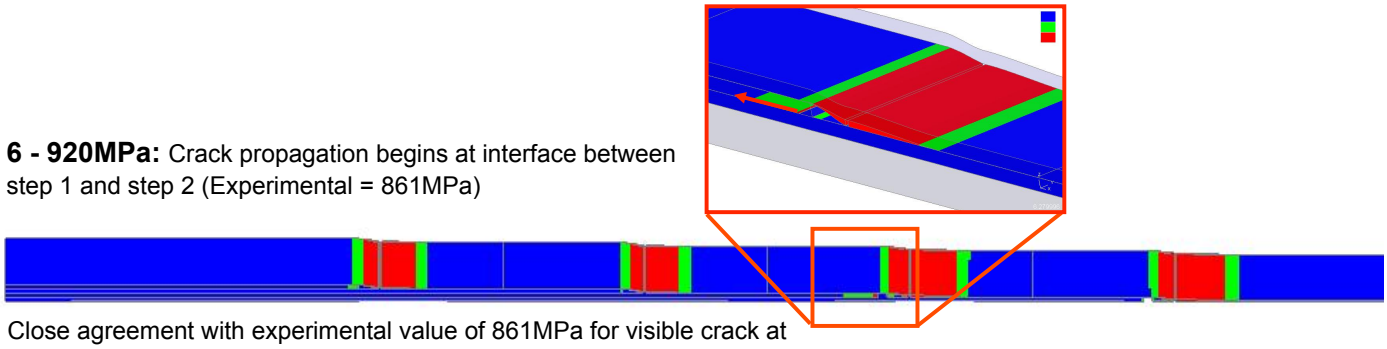

Close agreement with experimental value of 861MPa for visible crack at this location

7 - 1115MPa: Crack propagates in an unstable manner from end of step 2

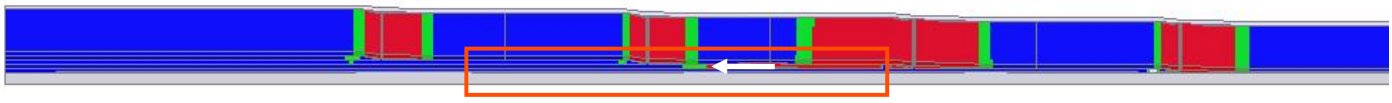

Experimental Failure Load = 1362MPa

Figure 16: Interfacial damage progression in the Single Cover Ply Specimen with G_{IC} = 0.85 N/mm (1mm defects included)

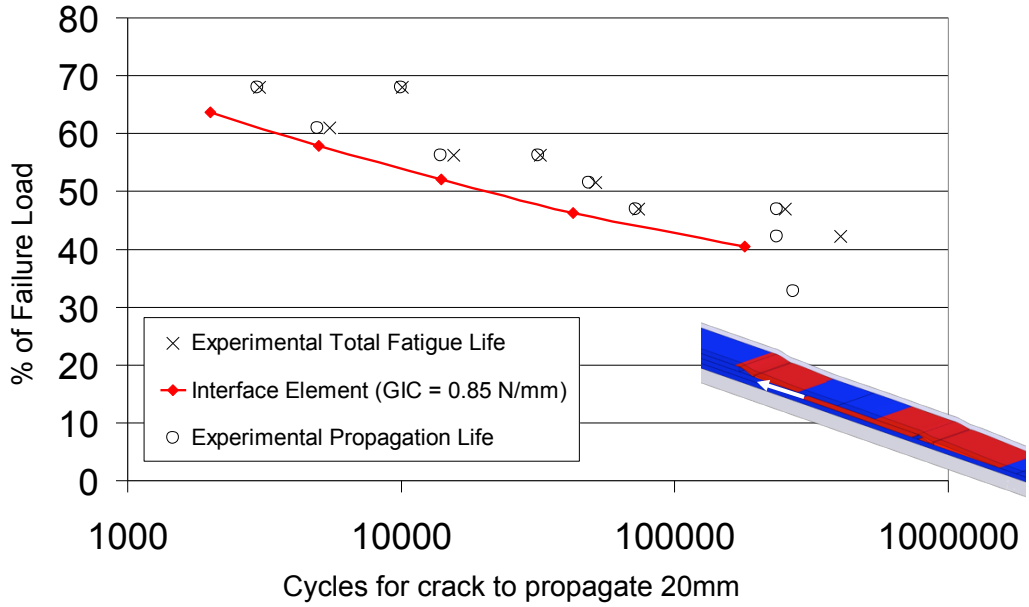

Figure 17: Cover ply specimen fatigue lives against normalised load level